



Ultrafine-Grained Two-Phase High-Entropy Alloy Microstructures Obtained via Recrystallization: Mechanical Properties

Ivan Guillot¹, Muriel Tyrman^{1,2}, Loic Perrière¹, Jean-Philippe P. Couzinié¹, Lola Liliensten³, Frédéric Prima³ and Guy Dirras^{2*}

¹ Univ Paris Est Creteil, CNRS, ICMPE (UMR 7182), Thiais, France, ² Université Sorbonne Paris Nord, CNRS, LSPM (UPR 3407), Villetaneuse, France, ³ PSL Research University, Chimie ParisTech, CNRS, Institut de Recherche de Chimie Paris, Paris, France

OPEN ACCESS

Edited by:

Zhefeng Zhang,
Institute of Metals Research
(CAS), China

Reviewed by:

Ruixiao Zheng,
Beihang University, China
Si Gao,
Kyoto University, Japan

*Correspondence:

Guy Dirras
dirras@univ-paris13.fr

Specialty section:

This article was submitted to
Structural Materials,
a section of the journal
Frontiers in Materials

Received: 25 February 2020

Accepted: 17 April 2020

Published: 27 May 2020

Citation:

Guillot I, Tyrman M, Perrière L, Couzinié J-PP, Liliensten L, Prima F and Dirras G (2020) Ultrafine-Grained Two-Phase High-Entropy Alloy Microstructures Obtained via Recrystallization: Mechanical Properties. *Front. Mater.* 7:125. doi: 10.3389/fmats.2020.00125

A metallurgical methodology has been set up in order to design alloys with improved mechanical properties such as strength–ductility trade-off, via improved strain hardening. To this end, a multi-concept approach including high-entropy alloys (HEAs), grain refinement, and chemical contrast and using the reversibility of the transformation-induced plasticity (TRIP) deformation mechanism has been implemented. The use of a conventional thermomechanical treatment involving cold rolling followed by an annealing stage at 650°C led to super-refined microstructures displaying an ultrafine-grained mixture (submicron size) of α (hcp) and β (bcc) phases. For Ti35Zr27.5Hf27.5Nb5Ta5 (Ti35-5-5), stress-induced martensitic transformation, and its subsequent reverse transformation during annealing at 650°C, led to a well-recrystallized state. A microstructure consisting of α and β equiaxed grains was obtained. Grain size is observed to increase within the submicron domain from about 300 to 600 nm with the holding time between 15 and 300 min. Contrariwise, for Ti35Zr26Hf26Nb6.5Ta6.5 (Ti35-6.5-6.5), which does not deform by the TRIP effect, the same thermomechanical treatment does not produce the recrystallization. Rather, precipitation of platelets in the recovered β matrix occurred. As for the mechanical properties, the yield strength of the alloys with dual-phase microstructure ranges between 950 and 1,150 MPa for Ti35-5-5 and between 850 and 950 MPa for Ti35-6.5-6.5, for annealing times ranging from 15 (higher yield strength) to 300 min (lower yield strength). This corresponds to a very large increase in the yield strength compared with that of the fully β alloys, displaying values of about 400 and 725 MPa for Ti35-5-5 and Ti35-6.5-6.5, respectively. Reasonable ductility was obtained for the alloys with optimized microstructures, which both display a tensile ductility of about 12% after annealing for 300 min at 650°C.

Keywords: high-entropy alloy, stress-induced martensitic transformation, recrystallization, ultrafine grains, mechanical properties

INTRODUCTION

It is clear that the strategy for the choice of a material results in compromise between optimal physical performances for the foreseen application and the capacities of shaping and mechanical strength required. Metals and metallic alloys are the fundamental structural materials. Their properties are strongly dependent not only on the chemical nature of the material but also on the initial microstructure and on its possible subsequent evolution under assigned loading or any external conditions to face. Consequently, it is of prior importance to control the elaboration process with an accurate enough understanding of how the elaboration acts on the microstructure and how the elaborated microstructure is next responsible for the final material behavior.

Ma (2003) suggested strategies allowing to get rid of the lack of ductility inherent to ultrafine-grained (UFG) metallic alloys, which are thought to be appealing materials thanks to their high strength. One strategy is based on processing materials with a bimodal grain size distribution. In the case of Cu, discussed in their work, the bimodal microstructures were obtained through severe plastic deformation (SPD) followed by heat treatment. Although interesting, this two-step strategy is not flexible because it does not allow a truly in-demand bimodal microstructure with a balanced volume fraction of each phase. Moreover, residual crystallographic texture resulting from the SPD-like step may also impact the subsequent mechanical behavior. It has to be noticed that the beneficial effect on improving ductility and toughness by recourse of bimodal grain size distributions has also been reported by Fan et al. (2006), Witkin et al. (2003), Billard et al. (2006), Langlois et al. (2019), Tingaud et al. (2019), Flipon et al. (2020), and García de la Cruz et al. (2020). A further step in optimizing the synergy between tensile strength and ductility has been introduced via the concept of harmonic structure design by Ameyama and Fujiwara (2012), Ota et al. (2014), Vajpai et al. (2016), and Dirras et al. (2017). Improved strain hardening rate due to delocalized plasticity from the coarse-grained core to the fine-grained shell and backstress contribution has been identified as the main mechanism of plasticity occurring in such heterogeneous materials. This is in line with a report by Lu (2014). In the main time, Liu et al. (2006) have used pulse electro-deposition method to tailor UFG Cu samples with controlled volume fraction of coherent twin boundaries. It was shown that the sample having a higher volume fraction of coherent as-grown twins exhibited both enhanced ductility and high strength (Dao et al., 2006). The same behavior was reported by Fellah et al. (2012) in the case of UFG Co processed via Hot Isostatic Pressing (HIP) via twinning-induced plasticity (TWIP)-like effect.

Thus, processing bulk sample exhibiting TWIP and/or transformation-induced plasticity (TRIP) mechanism have a huge potential for optimization of the mechanical properties, especially in terms of strength–ductility optimization. Indeed, the work of Sun et al. (2017) or Zhang et al. (2019) on titanium alloys confirmed this trend. Recently, Lilensten et al. (2017) proposed to combine the solid solution hardening brought by the high-entropy alloy (HEA) concept and the ductility and work-hardening characteristic of the TRIP Ti-alloy family. This study brought a proof of concept that combining these

two design approaches was a successful way to reach such mechanical properties. Combination of the TRIP mechanism with another classical metallurgy approach, the precipitation hardening, was also done by Lilensten et al. (2019) and Danard et al. (2019). These studies emphasize that several metallurgical design strategies can be used together to provide the best of each strategy's properties.

As a further development of the work of Lilensten et al. (2017), the present study proposes an innovative strategy to work out microstructures with controlled fine-grained Ti-rich $\alpha + \beta$. The synergy of the HEA concept, the UFG approach, the chemical contrast, and the TRIP mechanism is targeted to reach combination of superior strength and ductility. The developed methodology is expected to open on many other perspectives in terms of innovative microstructures and new physical and mechanical properties.

EXPERIMENTAL PROCEDURES

Sample Processing

The two alloys (Ti35-5-5 and Ti35-6.5-6.5) were produced by arc melting and induction furnace in an identical manner from slugs and wires of single metals with a purity of more than 99.9%. Two master alloys, NbTa and TiZrHf, were first produced by arc melting in an argon atmosphere on a cooled copper plate. A titanium getter was used prior each arc-melting fusion to capture the residual oxygen in the chamber. These master alloys were melted three times separately and then twice together. The alloys were then melted again twice in an induction furnace in a helium atmosphere in a cooled segmented copper crucible to obtain good homogenization by electromagnetic stirring. They were then shaped into ingots about 60 mm in length and 10 mm in diameter by arc melting. After the bottom and top of the ingot were cut to obtain two parallel faces, the alloys were cold rolled to a thickness reduction of 90% to produce a sheet with a thickness in the range of 0.8–1 mm. In order to obtain a two-phase α/β microstructure, the alloys were subsequently annealed in the two-phase region of the phase diagram (identified using ThermoCalc with the TCHEA1 database). Annealing was thus performed at 650°C between 15 and 300 min under helium. In addition, some samples were annealed in the β domain at 900°C for 30 min in order to reach a bcc single-phase microstructure.

Microstructural Characterization

Samples for microstructural characterizations were prepared by mechanical grinding using SiC paper up to grade 4,000 followed by a final polishing step of a minimum of 15 h using a vibrating table with 0.04- μm colloidal silica. The microstructural characterization was performed with Merlin Zeiss field emission scanning electron microscope (FE-SEM) coupled with an energy-dispersive X-ray spectrometer (EDS) and an electron backscatter diffraction (EBSD) detector from Oxford Instruments. Both detectors are driven by AZtec operating system. The secondary electron (SE) images and EBSD mappings were conducted at 25 kV, whereas the point EDS analyses were performed at 8 kV so that the interaction volume of the incident electrons was less than the size of the finest microstructure obtained for 15-min annealing at 650°C, using Ti K α , Zr L α , Hf M α , Nb L α , and Ta

$M\alpha$ peaks. For all the considered microstructures, the percentage of α and β phases of all the two-phase alloys was measured by image analysis using ImageJ software on 10 SE images at 5k of magnification, which corresponds to an analyzed surface area of 0.357 mm². Similarly, the chemical composition of the two phases was systematically determined by averaging 20 EDS measurements per phase, with the scatter corresponding to the standard deviation.

The fine structure analyses were analyzed using a JEOL 2000EX and a Tecnai F20 transmission electron microscope (TEM) both operating at 200 kV. Disk of 3 mm in diameter were thinned down to 100 μ m by manual polishing and then twin-jet electropolished using an electrolyte composed of a solution of HClO₄, butanol, and methanol, at -35°C and 15 V. The α and β grain size obtained for Ti35-5-5 after different annealing times at 650°C was measured manually on a hundred grains of each phase, corresponding to about 10 images in bright fields at 0 tilt and 50k of magnification. The dispersion corresponds to the standard deviation.

The crystal structure was characterized by X-ray diffraction (XRD) with a Panalytical X'Pert Pro MPD diffractometer in the Bragg-Brentano θ - θ configuration, using Co K α radiation ($\lambda = 0.178897$ nm) in a 2θ range from 20° to 135° .

Room Temperature Tensile Tests

Mechanical tensile testing was performed on dog-bone-shaped tensile specimens with a gauge length of 20 mm and a gauge width of 4 mm, which were machined in the annealed sheets (with a thickness of 0.8 mm) by electrical discharge machining. Tensile tests were performed at room temperature and at a strain

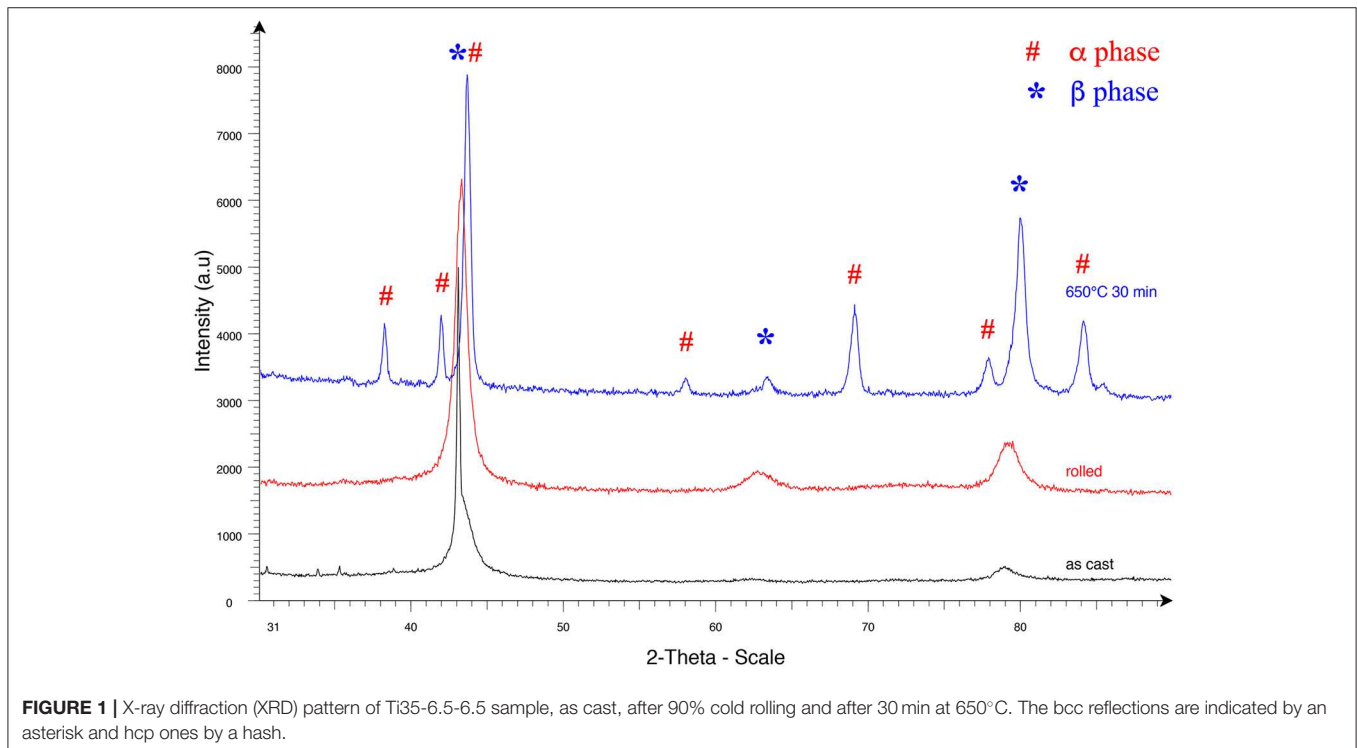
rate of 10^{-4} s^{-1} using a MTS Exceed[®] machine with a maximum force of 10 kN. The engineering strain was measured by an extensometer with 10-mm gauge length. Two samples were tested for each state. The yield strength, $R_{p0.2}$, was determined at 0.2% of plastic deformation offset.

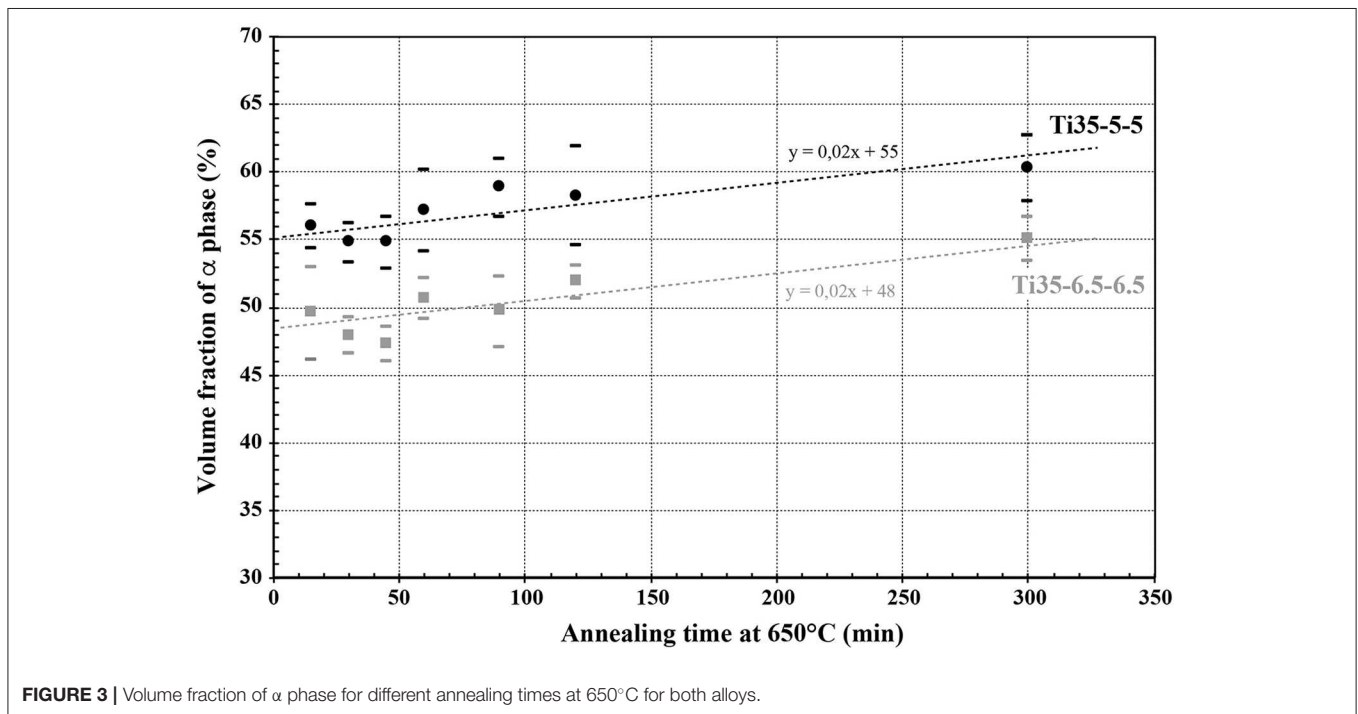
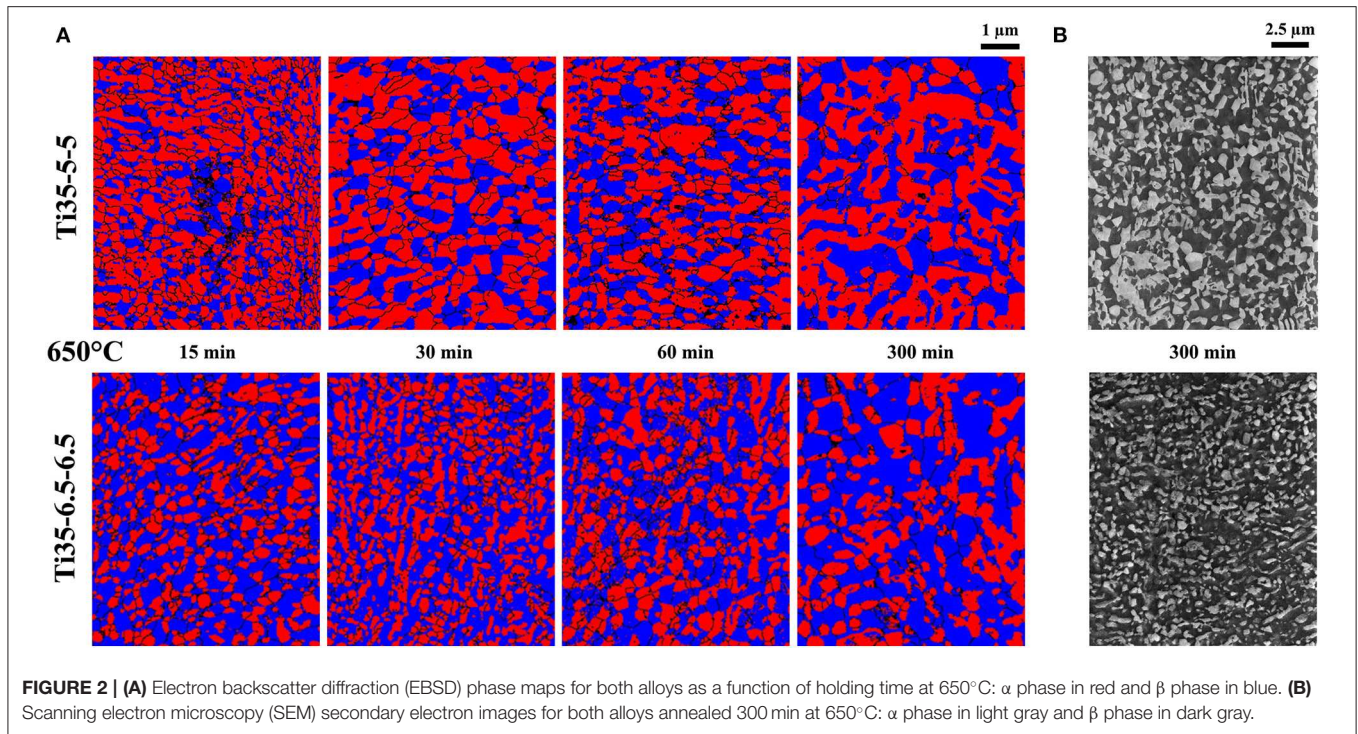
RESULTS AND DISCUSSION

Microstructure

A detailed characterization of the as-cast microstructure and deformation mechanisms of the Ti35-5-5 alloy was given elsewhere, with the alloy exhibiting an orthorhombic martensitic structure confirmed by XRD (Lilensten et al., 2014, 2017). After cold rolling and annealing in the β -domain, the alloy displays TRIP properties, which proceeds by martensitic transformation and fragmentation of the martensite laths (Lilensten et al., 2017). It can therefore be assumed that in the present case, cold rolling of the martensitic structure also proceeds by a further refinement of the microstructure. In contrast, for the Ti35-6.5-6.5 alloy, displaying a higher percentage of β -stabilizers (Nb and Ta), an as-cast bcc microstructure is retained even after 90% cold rolling (Figure 1), without any formation of stress-induced martensite. Owing to the extreme complexity of cold-rolled microstructures, only XRD was able to provide information on the present phases, at this stage of processing.

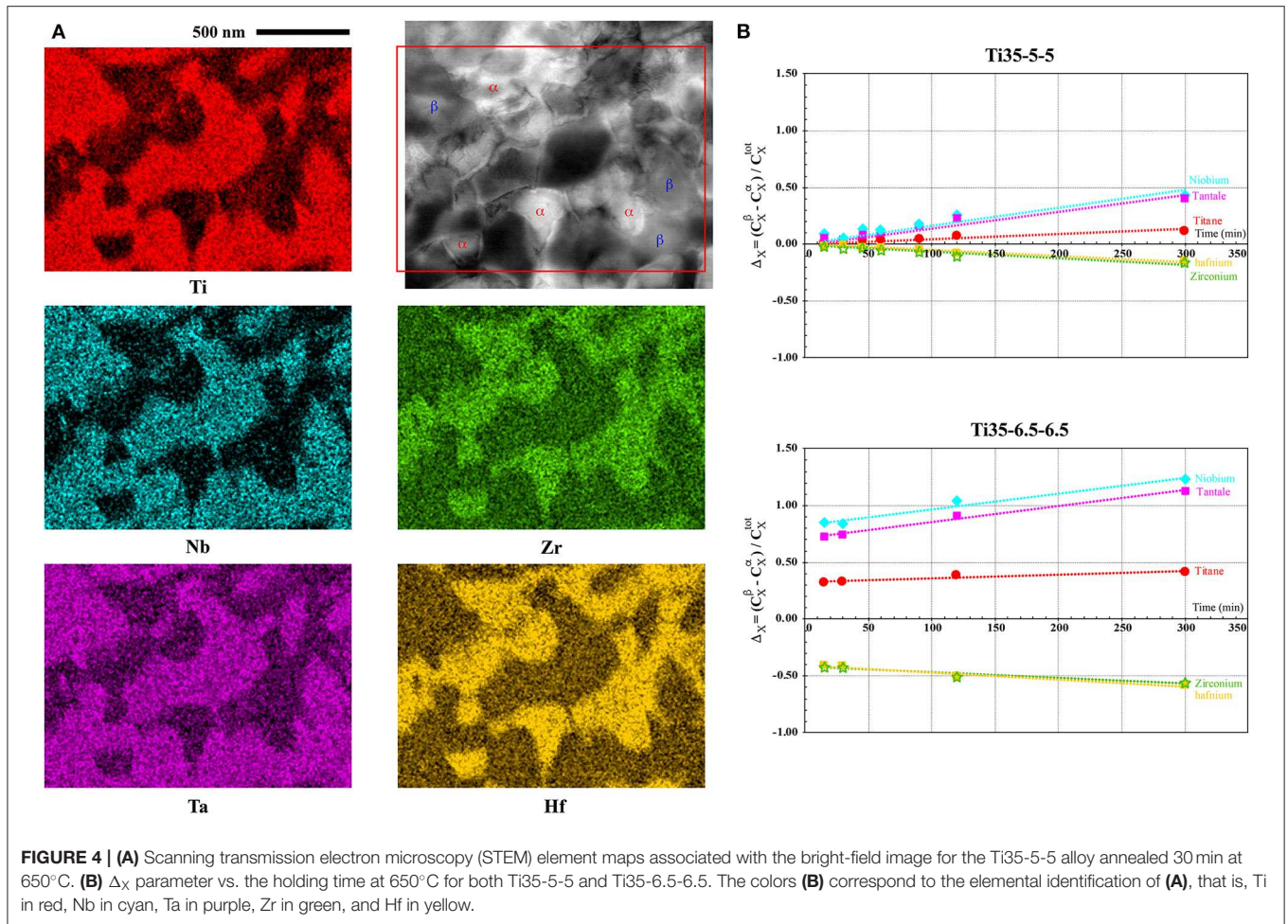
After cold rolling, annealing of the two alloys at 650°C in the two phases α/β domain was carried out for 15, 30, 45, 60, 90, 120, and 300 min. Diffraction patterns in Figure 1 confirm the α precipitation for a 30-min annealing at 650°C of the Ti35-6.5-6.5, displaying thus a dual-phase microstructure. Such





microstructure is confirmed for both Ti35-5-5 and Ti35-6.5-6.5 alloys by the EBSD analyses in **Figure 2A**, providing phase maps with α in red and β in blue, for selected annealing times. The secondary electron SEM images in **Figure 2B** show, after an annealing treatment of 300 min at 650°C, the dual-phase microstructures with the α phase in light gray and the β phase

in dark gray. On the one hand, independently of the alloys and the morphology of their microstructures, image analysis of SEM pictures at different annealing times shows that the percentage of alpha phase increases linearly with the holding time with the same slope for both alloys (**Figure 3**). The Ti35-6.5-6.5 alloy, which has the highest β -stabilizer content, naturally



has a lower content of α phase than Ti35-5-5. On the other hand, the observed increase in the percentage of α phase during annealing shows that thermodynamic equilibrium is not reached after 300 min (5 h). Moreover, Calphad calculations performed with the TCHEA4 database lead to 82.02 and 73.40% of α phase at equilibrium for Ti35-5-5 and Ti35-6.5-6.5 alloys, respectively. The difference of 8.64% between the two Calphad results is close to the gap of 7% between the two linear regressions in **Figure 3**.

A similar observation can be made on the partition of the elements in the two phases. The scanning transmission electron microscopy (STEM) element mapping of Ti, Zr, Hf, Nb, Ta, and the associated bright field in **Figure 4A** show a partition of the elements between the two phases. It can be seen that the α hexagonal phase is enriched in zirconium and hafnium whereas the concentrations of titanium, niobium, and tantalum increase in the β bcc phase.

The parameter Δ_X , equal to the ratio of the difference between the concentration of an element X measured by EDS in the β phase (C_X^β) to that measured in the α phase (C_X^α), relative to the nominal concentration of this element (C_X^{tot}) (Equation 1), is calculated for the various samples. As seen in **Figure 4B**, Δ_X displays once again a linear variation of Δ_X as a function of the

holding time for both alloys.

$$\Delta_X = \frac{(C_X^\beta - C_X^\alpha)}{C_X^{tot}} \text{ with } X = Ti, Zr, Hf, Nb, Ta \quad (1)$$

Whereas, the concentrations of the β elements Nb and Ta are higher and increase well in the β phase with annealing time, and the concentrations of Zr and Hf are higher in the α phase, the concentration of titanium remains greater in the β phase than in the α phase. These results are in qualitative agreement with the calculations performed using ThermoCalc and the TCHEA4 database performed at a slightly higher temperature than 650°C in order to have only the two predicted β bcc and α hcp phases.

Figures 5A,B show the bright-field TEM images of the two-phase microstructures for both alloys, at the same magnification and for the same annealing conditions as in **Figure 2A**. Ti35-5-5 alloy exhibits α and β equiaxed grains that grow with increasing holding time at 650°C from 290 ± 80 to 500 ± 130 nm for α and from 320 ± 85 to 590 ± 180 nm for β (**Figure 5A**). The grain size thus remains submicronic even during the longest holding time (300 min). The α and β grains most often exhibit between them the Burgers relationships well-established in the literature (Burgers, 1934): $\{111\}_\beta // \{11\bar{2}0\}_\alpha$, and $\{110\}_\beta // \{0001\}_\alpha$. These

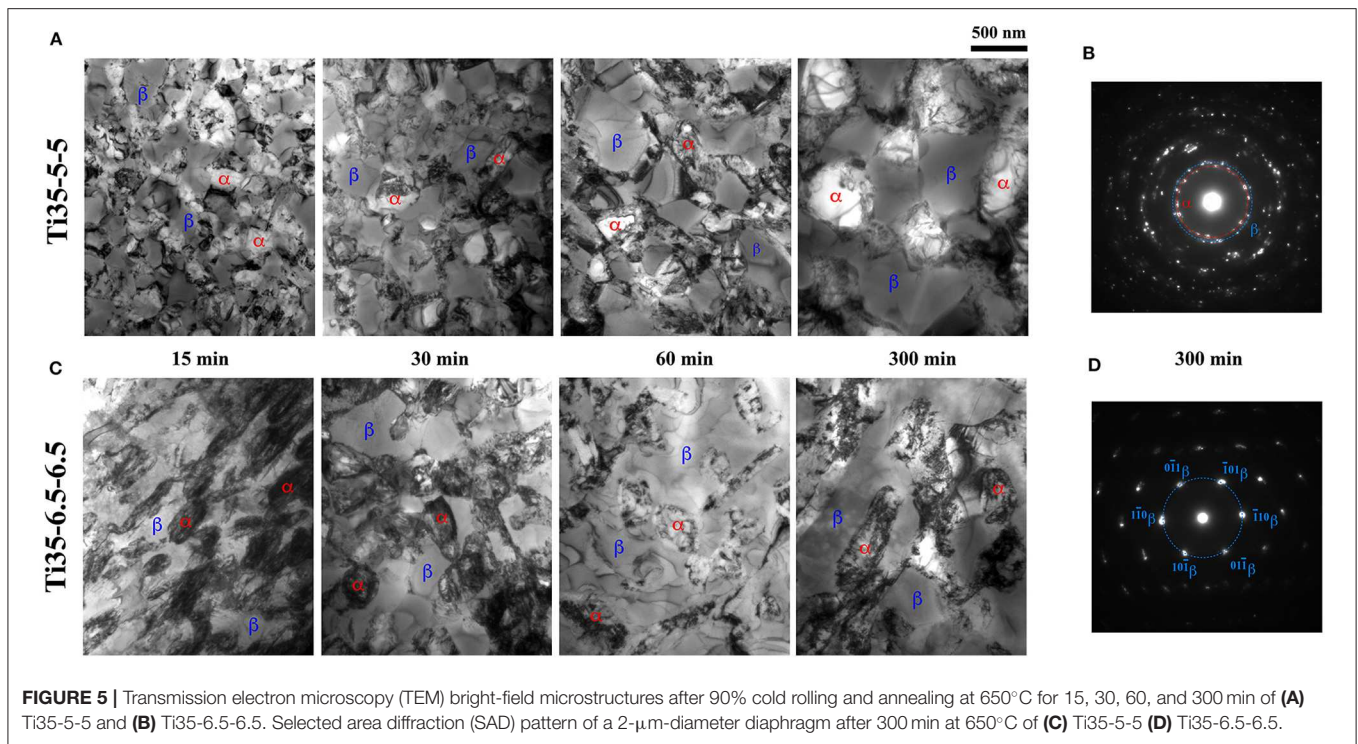


FIGURE 5 | Transmission electron microscopy (TEM) bright-field microstructures after 90% cold rolling and annealing at 650°C for 15, 30, 60, and 300 min of (A) Ti35-5-5 and (B) Ti35-6.5-6.5. Selected area diffraction (SAD) pattern of a 2- μm -diameter diaphragm after 300 min at 650°C of (C) Ti35-5-5 (D) Ti35-6.5-6.5.

relationships were further confirmed by plotting stereographic projections of neighboring α and β grains. In comparison, the microstructure of the Ti35-6.5-6.5 alloy looks totally different (Figure 5B). It is observed that the α precipitates have a platelet morphology, more or less elongated depending on the orientation of the mother phase β .

Selected area diffraction patterns using a 2- μm -diameter diaphragm are given in Figures 5C,D. For Ti35-5-5 (Figure 5C), numerous diffraction spots are observed, forming rings. Some, as highlighted by the blue ring, correspond to 110_{β} diffraction spots ($d_{110_{\beta}} = 0.241$ nm), whereas others correspond to α spots that lie a little close or further of this ring ($d_{1\bar{1}00_{\alpha}} = 0.273$ nm, $d_{0002_{\alpha}} = 0.255$ nm, and $d_{1\bar{1}01_{\alpha}} = 0.239$ nm), as suggested by the red circle on Figure 5C. This indicates that the submicronic microstructures given in Figure 5A are made of α and β grains with different orientation. For Ti35-6.5-6.5, the diffraction pattern provided in Figure 5D is made up of only a single zone axis of β phase: this shows that all the surrounding β matrices have the same orientation. The absence of α diffraction spots is only due to the fact that in the chosen conditions, the precipitates were not diffracting. In the case of Ti35-6.5-6.5 alloy, it can therefore be concluded that 90% cold rolling followed by annealing at 650°C does not appear to produce recrystallization of the microstructure, but rather recovery of the β grains that retain a grain size of at least 2 μm and precipitation of the α phase in the recovered matrix.

In summary, Ti35-5-5 heated to 650°C and held for 15 to 300 min forms a recrystallized microstructure of submicron $\alpha + \beta$ grains, whereas Ti35-6.5-6.5 has, for all holding times, a microstructure made of large β matrix of at least 2 μm , which

appears to be restored rather than recrystallized, in which plate-like α precipitates.

Thus, for Ti35-6.5-6.5 which contains the highest content of β -stabilizer, the mechanical energy stored in the form of dislocations during cold rolling is not sufficient to activate recrystallization at 650°C and leads instead to recovery of the β phase. In the case of the Ti35-5-5 alloy, the formation of fine martensite, the complex interaction between slip dislocations and this martensite during rolling, and the subsequent reversible transformation of the martensitic phase during annealing can be viewed as the main causes leading to recrystallization and to grain refinement to the nanoscale (Ma et al., 2005; Xu et al., 2006; Cai et al., 2011; Jiang et al., 2018).

As Figure 5A clearly shows, the grain size of the two phases α and β increases with holding time. Isothermal normal grain growth in pure metals and solid-solution alloys can be described approximately by the empirical model formulated by (Beck et al., 1947):

$$D = Kt^n \quad (2)$$

where D is the average grain size, t is the annealing time, and K and n are constants dependent on material and temperature, respectively, but independent of grain size. It is obvious that this relationship cannot hold for very short annealing periods, as the time required for recrystallization is no longer negligible (Burke, 1947; Gil and Planell, 1991). The equation for grain growth can then be expressed as follows:

$$D - D_0 = Kt^n \quad (3)$$

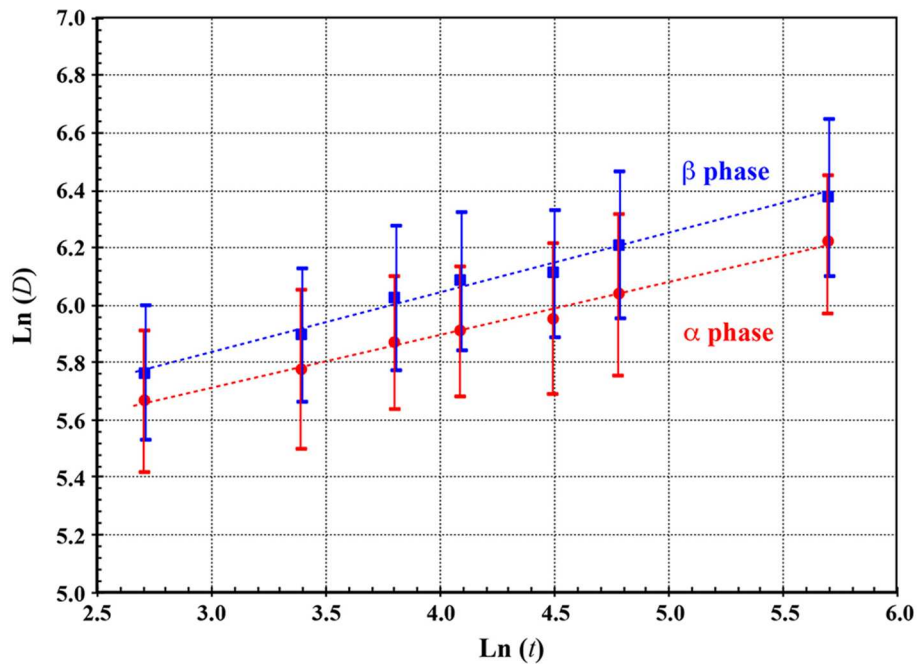


FIGURE 6 | Linear relationship between $\ln(D)$ and $\ln(t)$ for α and β grain growth of Ti35-5-5 at 650°C.

where D_0 is the initial grain size. With increasing annealing time, D_0 becomes negligible compared to D , so $D_0 \ll D$, and the growth law can be simplified as Equation (2) (Hu and Rath, 1970; Contieri et al., 2010). The calculated growth exponent, n , which is the slope of the linear relationship between $\ln D$ and $\ln t$ in **Figure 6**, is almost the same for the growth of α and β grains at 650°C, $n = 0.18$ and $n = 0.2$, respectively.

Hu et al. reported a set of grain growth data from the literature on the temperature dependence of n (Hu and Rath, 1970). It can be seen that in many cases, the value of n increases with temperature and approaches $n = 0.5$ near the melting point and for the high purity alloys. Besides, in general, the values of grain growth exponents for titanium and its alloys are high compared with those of other metals and alloys. For instance, the grain growth exponent for α titanium ranges from 0.30 at 700°C to 0.45 at 800°C. At temperatures above the β -*transus* (T 882°C), Gil et al. observed an increase in the growth exponent up to $n = 0.5$ (Gil and Planell, 2000). They explained this increase by the change in crystal structure from α (hcp) to β (bcc).

Wang et al. studied β grain growth at temperatures just above the β -*transus* for two titanium alloys, TG6 alloy (Ti-5.8Al-4.0Sn-4.0Zr-0.7Nb-1.5Ta-0.4Si-0.06C, wt.%), which is a near- α high-temperature titanium alloy and T17 alloy (Ti-5Al-4Mo-4Cr-2Sn-2Zr, wt.%), which belongs to near- β titanium alloy family, with β -*transus* temperatures of 1045°C and 895°C, respectively (Wang et al., 2011). The grain growth exponent n of these TG6 and T17 alloys ranges from 0.35 at 1055°C to 0.38 at 1075°C and from 0.27 at 905°C to 0.30 at 925°C, respectively. These values of n are lower than those of pure β titanium because these alloys have a high content of alloying elements, which slows

down the migration of the grain joints and thus the growth of the grains, known as the “solute drag effect” (Gil and Planell, 2000). Similarly, Lu et al. reported that the β grain growth exponents n for Ti-4Mo (900°C) and Ti-20Mo (800°C) alloys are 0.42 and 0.26, respectively. The lower grain growth exponent n for the Ti-20Mo alloy is again mainly due to the decrease in processing temperature and the increase in alloying element content (Lu et al., 2013).

The low values of the present study obtained for both α and β grain growth, respectively, 0.18 and 0.20, for Ti35-5-5 at 650°C (a temperature in the α/β two-phase domain) are consistent with the above values from the literature: the highly concentrated composition, which directly results from the HEA design approach, and the low annealing temperature, are parameters that lead to slow grain growth. However, it is mainly the presence of the two phases that strongly slows down grain growth and thus decreases the value of n : partition of the elements, namely, Ti, Nb, and Ta in the β bcc phase and Zr and Hf in the α hcp phase (**Figure 4**), is controlled by the diffusion rate, which is expected to be low for an annealing temperature of 650°C, close to $0.5T_f$, thus limiting the overall grain growth.

Mechanical Properties

The tensile true stress/true strain curves of Ti35-5-5 and Ti35-6.5-6.5 are plotted in **Figure 7**. The detailed tensile properties of specimens annealed at 650°C for different times are compared with those of fully β samples (30 min at 900°C) and summarized in **Tables 1, 2** for the alloy Ti35-5-5 and the alloy Ti35-6.5-6.5, respectively. With no surprise, the Young modulus depends on the microstructure. The Ti35-5-5 α/β alloy with nanoscale grains

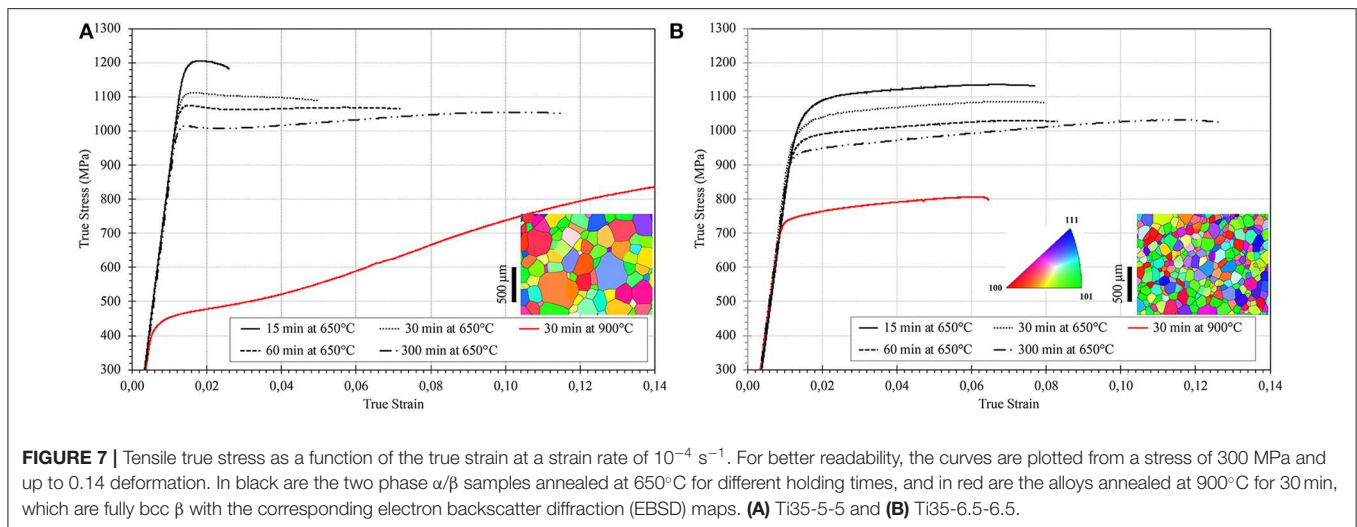


FIGURE 7 | Tensile true stress as a function of the true strain at a strain rate of 10^{-4} s^{-1} . For better readability, the curves are plotted from a stress of 300 MPa and up to 0.14 deformation. In black are the two phase α/β samples annealed at 650°C for different holding times, and in red are the alloys annealed at 900°C for 30 min, which are fully bcc β with the corresponding electron backscatter diffraction (EBSD) maps. **(A)** Ti35-5-5 and **(B)** Ti35-6.5-6.5.

TABLE 1 | Room temperature mechanical properties of Ti35-5-5 obtained from stress–strain engineering curves performed at a strain rate of 10^{-4} s^{-1} for different annealing times at 650°C and for 30 min at 950°C .

| Ti35-5-5 | Young modulus E (GPa) | Yield strength $R_{p0.2}$ (MPa) | Ultimate tensile strength (MPa) | Elongation | D_α | D_β |
|--------------------------------|----------------------------|------------------------------------|------------------------------------|------------|--------------------------|---------------------------|
| 15 min at 650°C | 85 | 1,178 | 1,185 | 0.014 | $290 \pm 78 \text{ nm}$ | $318 \pm 85 \text{ nm}$ |
| 30 min at 650°C | 86 | 1,090 | 1,095 | 0.086 | $322 \pm 102 \text{ nm}$ | $363 \pm 93 \text{ nm}$ |
| 60 min at 650°C | 87 | 1,056 | 1,060 | 0.120 | $368 \pm 92 \text{ nm}$ | $441 \pm 108 \text{ nm}$ |
| 300 min at 650°C | 86 | 998 | 1,002 | 0.157 | $504 \pm 128 \text{ nm}$ | $590 \pm 180 \text{ nm}$ |
| 30 min at 900°C | 79 | 430 | 760 | 0.260 | — | $170 \pm 100 \mu\text{m}$ |

Grain size evolution D_α and D_β are also shown.

has E value of about 86 GPa, slightly higher than that of the two-phase Ti35-6.5-6.5 alloy with a value close to 81 GPa. When annealed at 900°C for 30 min and subsequently water quenched, both alloys yielded Young moduli of ~ 79 GPa. This value is in line with that obtained by Lilensten et al. (2017). The variation in Young's modulus depends mainly on the volume fraction of the α and β phases. Indeed, the β phase is softer than the α phase, and the increase in its volume fraction results in a decrease in Young's modulus (Kuroda et al., 2019; Völker et al., 2019). Thus, Ti35-5-5 annealed at 650°C has a higher α phase fraction than Ti35-6.5-6.5 alloy and therefore exhibits a higher Young's modulus. Finally, the two alloys annealed in the β domain at 900°C display a lower Young's modulus than the dual-phase alloys.

For both alloys, the yield strength and the ultimate tensile strength decrease as the annealing time at 650°C increases while, at the same time, the ultimate elongation increases (Figure 7, Tables 1, 2). For the Ti35-5-5 alloy, it has been shown in Figures 5A, 6 that both α and β grain sizes increase with increasing holding time, which results in lower yield strength according to Hall and Petch's law. Similarly, Figure 5B shows that the plate-like α -precipitates in the β matrix increase in size during holding time, resulting in a decrease in yield strength and strengthening effect.

Additionally, for each holding time at 650°C , the yield strength of the Ti35-5-5 samples is systematically 100 to 200

TABLE 2 | Room temperature mechanical properties of Ti35-6.5-6.5 obtained from stress–strain engineering curves performed at a strain rate of 10^{-4} s^{-1} for different annealing times at 650°C and for 30 min at 950°C .

| Ti35-6.5-6.5 | Young modulus E (GPa) | Yield strength $R_{p0.2}$ (MPa) | Ultimate tensile strength (MPa) | Elongation |
|--------------------------------|----------------------------|------------------------------------|------------------------------------|------------|
| 15 min at 650°C | 80 | 1,020 | 1,070 | 0.086 |
| 30 min at 650°C | 83 | 990 | 1,030 | 0.081 |
| 60 min at 650°C | 81 | 955 | 975 | 0.107 |
| 300 min at 650°C | 81 | 920 | 936 | 0.132 |
| 30 min at 900°C | 79 | 730 | 763 | 0.058 |

MPa higher than that of the Ti35-6.5-6.5 samples. This is expected to be mainly due to the microstructure of the alloys. In Ti35-6.5-6.5, intragranular α precipitates are observed, which harden the alloy to a lesser extent than in Ti35-5-5 where the coexistence of smaller α and β grains enhances the deformation incompatibilities between grains and therefore the mechanical strengthening effect due to the α phase.

Finally, the tensile behavior of both alloys in their fully β bcc structure (in red in Figure 7) are completely different from that of the same alloys with dual-phase microstructure (in black

in **Figure 7**). The tensile behavior of the 100% β Ti35-5-5 alloy displays a marked stress-induced phase transformation effect, characterized by two distinct stages of the plastic domain of the tensile stress-strain curve, conferring the alloy with a very high work-hardening rate without loss of ductility (Lilensten et al., 2017). This alloy also has indeed a much larger ductility than Ti35-6.5-6.5, even though the β grain sizes are different (170 ± 100 and $90 \pm 50 \mu\text{m}$ for Ti35-5-5 and Ti35-6.5-6.5, respectively; **Figure 7**). Regarding Ti35-6.5-6.5, its tensile true stress-true strain curves do not show a TRIP effect and display moderate-to-low strain-hardening rate. One can note that a similar strain-hardening behavior is obtained for the fully β and for the α/β Ti35-6.5-6.5 samples. By analogy with the observations made on the equimolar alloy (Couzinié et al., 2015; Lilensten et al., 2018), the deformation modes should correspond to the dislocation slip, controlled in the early stages by the movement of the screw dislocations, the deformation being then rapidly localized in bands.

The tensile true stress-strain curves of the dual-phase Ti35-5-5 alloy show an increase in ductility with increasing annealing time. In addition, the shape of the tensile curves suggests that the TRIP deformation mechanism also appears to be effective for the recrystallized β grains of two-phase alloys. Indeed, at least for holding times above 60 min, a plateau is observed at the beginning of the plastic deformation, followed by a stress increase for larger strains. For shorter aging times, the strong contrasts observed in the TEM bright-field images in **Figure 5A** suggest the presence of significant internal stresses, especially in the α phase, which may reduce ductility. The reduction in grain size and the high internal stresses between grains associated with chemical partitioning during α precipitation, which stabilizes the β phase, may also inhibit the initiation of the TRIP effect.

Overall, the mechanical results can be summarized as follows:

- Whereas fully β Ti35-6.6-6.5 alloy exhibits a higher yield strength than Ti35-5-5 alloy, an opposite trend is observed in the case of the dual-phase microstructures. Indeed, Ti35-5-5 systematically displays a larger yield strength than does Ti35-6.5-6.5, for a similar thermomechanical treatment.
- More specifically, the yield strength of the alloys with dual-phase microstructure lies between 950 and 1,150 MPa for Ti35-5-5 and between 850 and 950 MPa for Ti35-6.5-6.5 for annealing times from 15 min (higher yield strength) to 300 min (lower yield strength).
- Annealing for 300 min at 650°C leads to a tensile ductility of about 12% for both alloys compositions.
- The two-phase Ti35-5-5 alloy, in particular for the longest annealing time that leads to the largest α and β grains of about 500 nm, seems to retain a TRIP deformation mode, although it is weakly marked on the tensile curves.
- The ductility of the Ti35-5-5 alloy increased continuously with increasing holding time at 650°C, contrarily to the Ti35-6.5-6.5 counterpart whose ductility remains constant for the 15-, 30-, and 60-min treatment at 650°C. Only the 300 min/650°C treatment leads to an increase of ductility for this alloy, probably thanks to minimized internal stresses resulting from phase contrast.

CONCLUSIONS

The influence of thermo-mechanical treatments was studied for two HEAs. Combining cold rolling with annealing treatments at various times at 650°C resulted in distinct behaviors for the two alloys Ti35-5-5 and Ti35-6.5-6.5, in spite of their close compositions. For Ti35-5-5, the cold rolling of the initial martensite structure leads to an intense fragmentation of the grains. After the reversion of the martensite during annealing at 650°C in the two-phase domain of the phase diagram, an important nucleation of beta grains was generated and further led to observed submicron alpha and beta grain microstructure. In the case of Ti35-6.5-6.5, which does not deform by the TRIP effect, the mechanical energy stored in the alloy during cold rolling is not sufficient to trigger recrystallization. Instead, during annealing, recovery of the beta phase and intragranular precipitation of the alpha phase platelets occurred. Therefore, it can be concluded that the stress-induced martensite transformation and the subsequent reverse transformation are essential to produce the nanograins.

Overall, this study demonstrates that dual-phase submicron grains with α (hcp) and β (bcc) structure can be produced solely with the use of conventional thermomechanical treatment on two HEAs. This elaboration strategy makes it possible to combine the so-called cocktail effect inherent to the HEA concept, with grain refinement and chemical contrast. Tensile testing results finally show how thermal treatments can thus be used to tune the mechanical properties and especially the yield strength, for both alloys. Adjusting the alloy composition, the temperature, or annealing time allows for further microstructure tailoring.

DATA AVAILABILITY STATEMENT

All datasets generated for this study are included in the article/supplementary material.

AUTHOR CONTRIBUTIONS

IG analyzed the microstructure, assembled the results, and wrote the draft. MT carried out part of the microstructure observations. LP prepared the HEA alloys and performed the thermomechanical treatments. J-PC and LL discussed the mechanical tests and confronted the microstructures. FP and GD discussed and corrected the manuscript. GD initiated the project behind the work presented here.

FUNDING

The French ANR (Agence Nationale de la Recherche) and CGI (Commissariat à l'Investissement d'Avenir) are gratefully acknowledged for their financial support of this work through grants ANR-10-LABX-0096 and ANR-18-IDEX-0001.

ACKNOWLEDGMENTS

The authors would also like to thank Rémy Pirès and Julie Bourgon from ICMPE for their assistance in the analyses and experiments performed with the SEM, TEM, and STEM.

REFERENCES

- Ameyama, K., and Fujiwara, H. (2012). Creation of harmonic structure materials with outstanding mechanical properties. *Mater. Sci. Forum* 706–709, 9–16. doi: 10.4028/www.scientific.net/MSF.706-709.9
- Beck, P. A., Joseph, C., Kremer, J. C., and Demer, L. (1947). Grain growth in high purity aluminium. *Phys. Rev.* 71:555. doi: 10.1103/PhysRev.71.555
- Billard, S., Fondère, J. P., Bacroix, B., and Dirras, G. F. (2006). Macroscopic and microscopic aspects of the deformation and fracture mechanisms of ultrafine-grained aluminum processed by hot isostatic pressing. *Acta Materialia* 54, 411–421. doi: 10.1016/j.actamat.2005.09.012
- Burgers, W. G. (1934). On the process of transition of the cubic-body-centered modification into the hexagonal-close-packed modification of zirconium. *Physica I* 1, 561–586. doi: 10.1016/S0031-8914(34)80244-3
- Burke, J. E. (1947). Grain growth in alpha-brass. *J. Appl. Phys.* 18:1028. doi: 10.1063/1.1697574
- Cai, M. H., Lee, C. Y., Kang, S., and Lee, Y. K. (2011). Fine-grained structure fabricated by strain-induced martensite and its reverse transformations in a metastable β titanium alloy. *Scripta Materialia* 64, 1098–1101. doi: 10.1016/j.scriptamat.2011.02.030
- Contieri, R. J., Zanolto, M., and Caram, R. (2010). Recrystallization and grain growth in highly cold worked CP-Titanium. *Mater. Sci. Eng. A* 527, 3994–4000. doi: 10.1016/j.msea.2010.03.023
- Couzinié, J. P., Lilensten, L., Champion, Y., Dirras, G., Perrière, L., and Guillot, I. (2015). On the room temperature deformation mechanisms of a TiZrHfNbTa refractory high-entropy alloy. *Mater. Sci. Eng. A* 645, 255–263. doi: 10.1016/j.msea.2015.08.024
- Danard, Y., Poulain, R., Garcia, M., Guillou, R., Thiaudière, D., Mantri, S., et al. (2019). Microstructure design and *in-situ* investigation of TRIP/TWIP effects in a forged dual-phase Ti-10V-2Fe-3Al alloy. *Materialia* 8:100507. doi: 10.1016/j.mta.2019.100507
- Dao, M., Lu, L., Shen, Y. F., and Suresh, S. (2006). Strength, strain-rate sensitivity and ductility of copper with nanoscale twins. *Acta Materialia* 54, 5421–5432. doi: 10.1016/j.actamat.2006.06.062
- Dirras, G., Ueda, D., Hocini, A., Tingaud, D., and Ameyama, K. (2017). Cyclic shear behavior of conventional and harmonic structure-designed Ti-25Nb-25Zr β -titanium alloy: back-stress hardening and twinning inhibition. *Scripta Materialia* 138, 44–47. doi: 10.1016/j.scriptamat.2017.05.033
- Fan, G. J., Choo, H., Liaw, P. K., and Lavernia, E. J. (2006). Plastic deformation and fracture of ultrafine-grained Al-Mg alloys with a bimodal grain size distribution. *Acta Materialia* 54, 1759–1766. doi: 10.1016/j.actamat.2005.11.044
- Fellah, F., Schoenstein, F., Dakhlaoui-Omrani, A., Chérif, S. M., Dirras, G., and Jouini, N. (2012). Nanostructured cobalt powders synthesised by polyol process and consolidated by spark plasma sintering: microstructure and mechanical properties. *Mater. Charac.* 69, 1–8. doi: 10.1016/j.matchar.2012.03.017
- Flipon, B., Keller, C., Quey, R., and Barbe, F. (2020) A full-field crystal-plasticity analysis of bimodal polycrystals. *Int. J. Solids Struct.* 184, 178–192. doi: 10.1016/j.ijsolstr.2019.02.005
- García de la Cruz, L., Martínez, M., Keller, C., and Hug, E. (2020) Achieving good tensile properties in ultrafine grained nickel by spark plasma sintering. *Mater. Sci. Eng. A* 772:138770. doi: 10.1016/j.msea.2019.138770
- Gil, F. J., and Planell, J. A. (1991). Growth order and activation energies for grain growth of Ti-6Al-4V alloy in β phase. *Scripta Metall. Materialia* 25, 2843–2848. doi: 10.1016/0956-716X(91)90167-Y
- Gil, F. J., and Planell, J. A. (2000). Behaviour of normal grain growth kinetics in single phase titanium and titanium alloys. *Mater. Sci. Eng. A* 283, 17–24. doi: 10.1016/S0921-5093(00)00731-0
- Hu, H., and Rath, B. B. (1970). On the time exponent in isothermal grain growth. *Metall. Trans.* 1, 3181–3184.
- Jiang, X. J., Zhao, H. T., Han, R. H., Zhang, X. Y., Ma, M. Z., and Liu, R. P. (2018). Grain refinement and tensile properties of a metastable TiZrAl alloy fabricated by stress-induced martensite and its reverse transformation. *Mater. Sci. Eng. A* 722, 8–13. doi: 10.1016/j.msea.2018.02.104
- Kuroda, P. A. B., Quadros, F. D., de Araujo, R. O., Afonso, C. R. M., and Grandini, C. R. (2019). Effect of thermomechanical treatments on the phases, microstructure, microhardness and young's modulus of Ti-25Ta-Zr alloys. *Materials* 12:3210. doi: 10.3390/ma12193210
- Langlois, P., Tingaud, D., and Dirras, D. (2019). “Spark plasma sintering as a route for producing in-demand microstructures: application to the tensile-ductility enhancement of polycrystalline nickel,” in *Spark Plasma Sintering of Materials*, ed P. Cavaliere (Cham: Springer), 575–604. doi: 10.1007/978-3-030-05327-7_20
- Lilensten, L., Couzinié, J. P., Bourgon, J., Perrière, L., Dirras, G., Prima, F., et al. (2017). Design and tensile properties of a bcc Ti-rich high-entropy alloy with transformation-induced plasticity. *Mater. Res. Lett.* 5, 110–116. doi: 10.1080/21663831.2016.1221861
- Lilensten, L., Couzinié, J. P., Perrière, L., Bourgon, J., Emery, N., and Guillot, I. (2014). New structure in refractory high-entropy alloys. *Mater. Lett.* 132, 123–125. doi: 10.1016/j.matlet.2014.06.064
- Lilensten, L., Couzinié, J. P., Perrière, L., Hocini, A., Keller, C., Dirras, G., et al. (2018). Study of a bcc multi-principal element alloy: tensile and simple shear properties and underlying deformation mechanisms. *Acta Materialia* 142, 131–141. doi: 10.1016/j.actamat.2017.09.062
- Lilensten, L., Danard, Y., Brozek, C., Mantri, S., Castany, P., Gloriant, T., et al. (2019). On the heterogeneous nature of deformation in a strain-transformable beta metastable Ti-V-Cr-Al alloy. *Acta Materialia* 162, 268–276. doi: 10.1016/j.actamat.2018.10.003
- Liu, L. X., Chen, X. H., and Lu, L. (2006). Strain rate sensitivity of ultrafine-grained Cu with nanosized twins, *Acta Metallurgica Sinica* 19, 313–318. doi: 10.1016/S1006-7191(06)62067-X
- Lu, J. W., Zhao, Y. Q., Ge, P., and Niu, H. Z. (2013). Microstructure and beta grain growth behavior of Ti-Mo alloys solution treated. *Mater. Charac.* 84, 105–111. doi: 10.1016/j.matchar.2013.07.014
- Lu, K. (2014). Making strong nanomaterials ductile with gradients. *Science* 345, 1455–1456. doi: 10.1126/science.1255940
- Ma, E. (2003). Instabilities and ductility of nanocrystalline and ultrafine-grained metals, *Scripta Materialia* 49, 663–668. doi: 10.1016/S1359-6462(03)00396-8
- Ma, Y., Jin, J. E., and Lee, Y. K. (2005). A repetitive thermomechanical process to produce nano-crystalline in a metastable austenitic steel. *Scripta Materialia* 52, 1311–1315. doi: 10.1016/j.scriptamat.2005.02.018
- Ota, M., Shimojo, K., Okada, S., Vajpai, S. K., and Ameyama, K. (2014). Harmonic structure design and mechanical properties of pure ni compact. *J. Powder Metall. Min.* 3:1000122. doi: 10.4172/2168-9806.1000122
- Sun, F., Zhang, J. Y., Vermaut, P., Choudhuri, D., Alam, T., Mantri, S. A., et al. (2017). Strengthening strategy for a ductile metastable β -titanium alloy using low-temperature aging. *Mater. Res. Lett.* 5, 547–553. doi: 10.1080/21663831.2017.1350211
- Tingaud, D., Sadatn, T., and Dirras, D. (2019). “Nickel-tungsten composite-like microstructures processed by spark plasma sintering for structural applications” in *Spark Plasma Sintering of Materials*, ed P. Cavaliere (Cham: Springer), 604–634. doi: 10.1007/978-3-030-05327-7_21
- Vajpai, S. K., Sawangrat, C., Yamaguchi, O., Ciuca, O. P., and Ameyama, K. (2016). Effect of bimodal harmonic structure design on the deformation behavior and mechanical properties of Co-Cr-Mo alloy. *Mater. Sci. Eng. C* 58, 1008–1015. doi: 10.1016/j.msec.2015.09.055
- Völker, B., Maier-Kiener, V., Werbach, K., Müller, T., Pilz, S., Calin, M., et al. (2019) Influence of annealing on microstructure and mechanical properties of ultrafine-grained Ti45Nb. *Mater. Des.* 179:107864. doi: 10.1016/j.matdes.2019.107864
- Wang, T., Guo, H., Tan, L., Yao, Z., and Zhao, Y., Liu, P. (2011). Beta grain growth behavior of TG6 and Ti17 titanium alloys. *Mater. Sci. Eng. A* 528, 6375–6380. doi: 10.1016/j.msea.2011.05.042

- Witkin, D., Lee, Z., Rodriguez, R., Nutt, S., and Lavernia, E. (2003). Al-Mg alloy engineered with bimodal grain size for high strength and increased ductility. *Scripta Materialia* 49, 297–302. doi: 10.1016/S1359-6462(03)00283-5
- Xu, W., Kim, K. B., Das, J., Calin, M., Rellinghaus, B., and Eckert, J. (2006). Deformation-induced nanostructuring in a Ti-Nb-Ta-In alloy. *Appl. Phys. Lett.* 89:031906. doi: 10.1063/1.2222239
- Zhang, J., Sun, F., Chen, Z., Yang, Y., Shen, B., Li, J., et al. (2019). Strong and ductile beta Ti-18Zr-13Mo alloy with multimodal twinning. *Mater. Res. Lett.* 7, 251–257. doi: 10.1080/21663831.2019.1595763

Conflict of Interest: The authors declare that the research was conducted in the absence of any commercial or financial relationships that could be construed as a potential conflict of interest.

Copyright © 2020 Guillot, Tyrman, Perrière, Couzinié, Lilensten, Prima and Dirras. This is an open-access article distributed under the terms of the Creative Commons Attribution License (CC BY). The use, distribution or reproduction in other forums is permitted, provided the original author(s) and the copyright owner(s) are credited and that the original publication in this journal is cited, in accordance with accepted academic practice. No use, distribution or reproduction is permitted which does not comply with these terms.